IARJSET ISSN (O) 2393-8021, ISSN (P) 2394-1588

International Advanced Research Journal in Science, Engineering and Technology

Impact Factor 8.311 ⁜ Peer-reviewed & Refereed journal ⁜ Vol. 13, Issue 5, May 2026

DOI: 10.17148/IARJSET.2026.13540

Implementation of HMI-Based Gesture Recognition and UWB Radar in Autonomous Vehicles

Shrisanjaykumaar K[1], Dr. O. Saraniya[2]

Dept. of Electronics and Communication Engg, Government College of Technology Coimbatore, India[1]

Professor (CAS), Dept. of ECE, Government College of Technology Coimbatore, India[2]

Abstract: This paper presents the MATLAB simulation and implementation of a 2–6 GHz CMOS Ultra-Wideband (UWB) radar transceiver front-end designed in 45 nm technology for HMI-based gesture recognition in autonomous vehicles. The transmitter chain employs digital pulse generation (5 ns rectangular pulse), Gaussian pulse shaping for spectral compliance, a Digitally Controlled Oscillator (DCO) providing a 4 GHz carrier, and an up-conversion mixer producing an RF output at 4.5 GHz. The received signal is processed via matched-filter correlation for range estimation, CA-CFAR detection for robust target identification, and a Kalman-filter-based tracker for long-range target following. An 8-gesture recognition vocabulary is implemented, with each gesture mapped to a specific vehicle command. Simulation results confirm FCC Part 15 UWB spectral compliance, accurate range detection at 45.5 m, multi-target resolution of pedestrian-car scenarios at 30–32 m separation, and gesture detection with a sub-5 ns observation window. The system achieves low-power, integrated radar-based HMI suitable for next-generation autonomous vehicles.

Index Terms: UWB radar, gesture recognition, autonomous vehicles, CMOS transceiver, CFAR detection, Kalman tracking, HMI, FCC compliance.

I. INTRODUCTION

Autonomous vehicles (AVs) demand reliable, low-latency human–machine interfaces (HMI) that operate under diverse environmental conditions including low-light, fog, and rain. Camera-based systems suffer from privacy concerns, illumination dependency, and computational overhead. Capacitive touch-based interfaces require physical contact and introduce latency. Ultra-Wideband (UWB) radar, operating in the 2–6 GHz band, offers a compelling alternative: it provides centimetre-level range accuracy, operates through non-metallic materials, and consumes milliwatt-scale power when implemented in nanoscale CMOS.

This work presents a complete MATLAB simulation of a 45 nm CMOS UWB radar transceiver for gesture-based vehicle control. The system covers the full signal processing chain from digital pulse generation and FCC-compliant spectral shaping, through up-conversion, free-space propagation, noise modelling, matched-filter correlation, CA-CFAR detection, Kalman-filter tracking, to final gesture classification. The 8-gesture command vocabulary is directly mapped to critical vehicle actions including steering, acceleration, braking, and mode selection.

The rest of this paper is organised as follows: Section II reviews related work. Section III describes the transceiver architecture. Section IV presents the transmitter implementation. Section V details the receiver and signal processing chain. Section VI discusses gesture recognition. Section VII presents simulation results. Section VIII concludes the paper.

II. RELATED WORK

Wang et al. [1] demonstrated a 3–10 GHz UWB front-end transceiver in 0.13 µm CMOS targeting biomedical radar with a noise figure of 4.5 dB and power consumption below 30 mW. The same group reported a receiver low-noise amplifier (LNA) in the same process node achieving 9 dB gain over a matched bandwidth of 7 GHz [2]. Bevilacqua and Niknejad [3] presented a wideband CMOS LNA for 3.1–10.6 GHz with 9.3 dB gain and 2.5 dB noise figure, establishing a baseline for CMOS wideband low-noise design. More recently, Tharakan et al. [4] reported a 2–6 GHz CMOS transceiver for automotive radar in 65 nm CMOS consuming 50 mW total DC power.

Gesture recognition using radar has been explored extensively at mmWave frequencies (60 GHz and 77 GHz), but sub-6 GHz UWB radar remains attractive for its superior penetration through automotive cabin materials, lower cost, and

IARJSET ISSN (O) 2393-8021, ISSN (P) 2394-1588

International Advanced Research Journal in Science, Engineering and Technology

Impact Factor 8.311 ⁜ Peer-reviewed & Refereed journal ⁜ Vol. 13, Issue 5, May 2026

DOI: 10.17148/IARJSET.2026.13540

compatibility with legacy CMOS nodes. The combination of a miniaturised CMOS UWB transceiver with robust signal processing (correlation, CFAR, Kalman filtering) represents the current state of the art for in-cabin HMI applications.

III. SYSTEM ARCHITECTURE

The proposed transceiver consists of a transmitter chain and a receiver chain implemented entirely in MATLAB/Simulink for functional verification prior to CMOS layout. The block-level architecture is shown in Fig. 1 (transmitter) and described in subsequent sections.

A. Transmitter Chain

The transmitter generates 5 ns rectangular pulses at a pulse repetition frequency (PRF) determined by the desired unambiguous range. Each pulse undergoes Gaussian shaping to attenuate spectral sidelobes, followed by up-conversion to the 2–6 GHz RF band using a DCO-driven mixer. The RF output is then power-amplified and radiated.

B. Receiver Chain

The receiver implements a direct-conversion architecture. After low-noise amplification, the received signal is correlated with the known transmitted waveform (matched filtering). The correlation output is passed to a CA-CFAR detector for range bin evaluation, and confirmed detections are fed into a Kalman filter tracker for smooth trajectory estimation. Gesture classification is performed on the extracted range-time signature.

IV. TRANSMITTER IMPLEMENTATION

A. Digital Pulse Generator

A rectangular pulse of 5 ns width and unit amplitude is generated digitally. In the frequency domain this produces an ideal sinc spectrum with strong, widely spaced sidelobes as shown in Fig. 1. The wide spectral spread of the rectangular pulse makes it non-compliant with FCC Part 15 UWB limits and necessitates pulse shaping in the following stage.

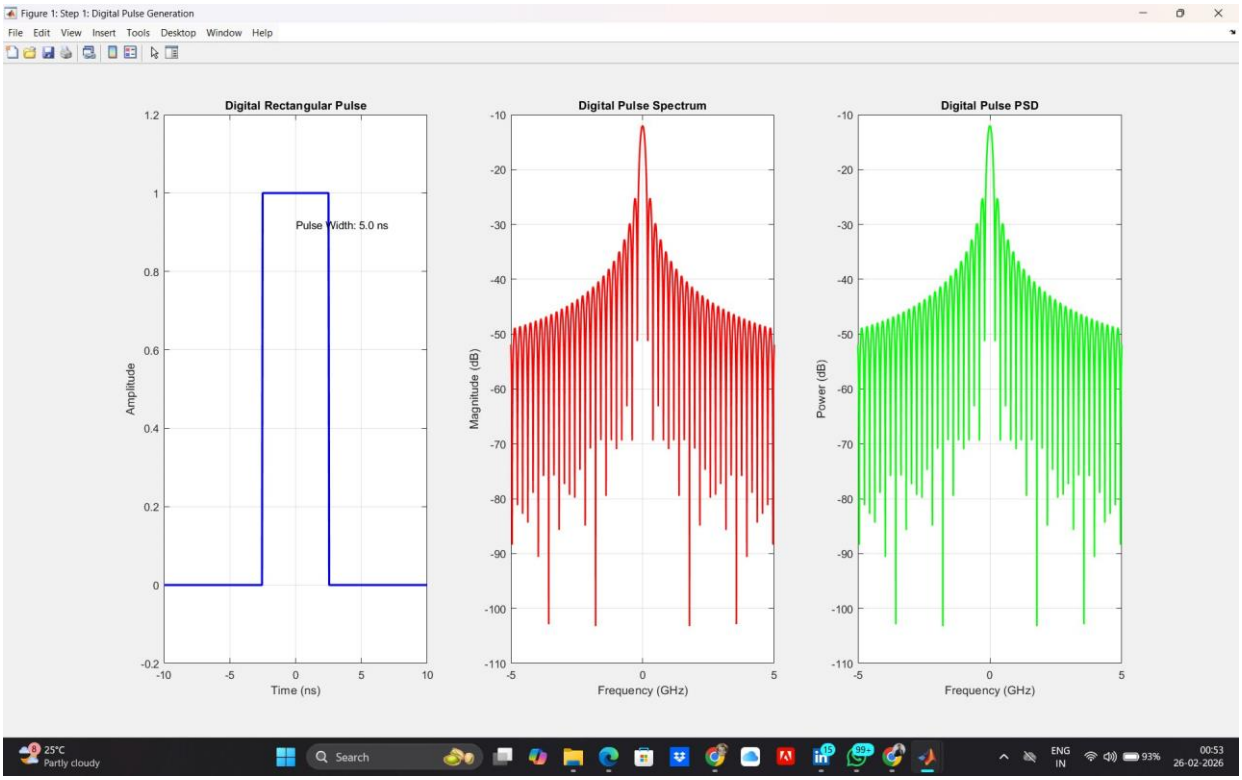

Fig. 1. Digital pulse generator output: rectangular pulse (5 ns width) in time domain and corresponding sinc spectrum.

B. Gaussian Pulse Shaping

The rectangular pulse is convolved with a Gaussian filter kernel, transforming the sharp transitions into a smoothly varying bell-shaped waveform. The resulting spectrum is compact with rapidly decaying sidelobes, as shown in Fig. 2. This is the primary step achieving FCC compliance by concentrating signal energy within the permitted spectral mask.

IARJSET ISSN (O) 2393-8021, ISSN (P) 2394-1588

International Advanced Research Journal in Science, Engineering and Technology

Impact Factor 8.311 ⁜ Peer-reviewed & Refereed journal ⁜ Vol. 13, Issue 5, May 2026

DOI: 10.17148/IARJSET.2026.13540

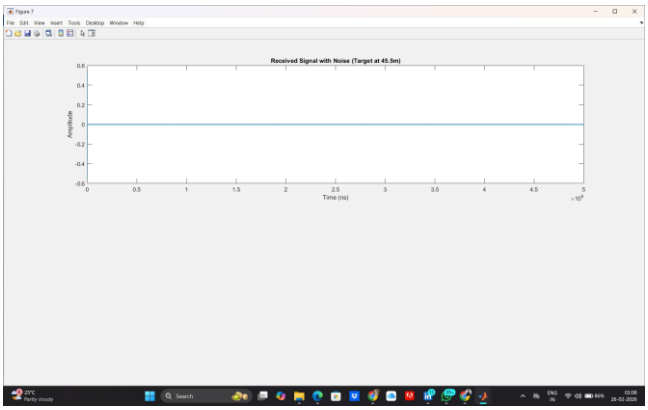

Fig. 2. Gaussian pulse shaping: bell-shaped waveform (time domain) and compact spectrum with attenuated sidelobes.

C. Digitally Controlled Oscillator

The DCO produces a continuous 4 GHz sinusoidal carrier. Its simulated frequency-domain representation shows a sharp spectral peak at the carrier frequency surrounded by noise skirts indicative of phase noise. Low phase noise is critical for clutter rejection in automotive environments.

D. Up-Conversion Mixer

The Gaussian-shaped pulse (IF = 500 MHz) is mixed with the DCO output (LO = 4 GHz), producing a burst of high-frequency RF oscillations centred at 4.5 GHz as shown in Fig. 3. The mixer achieves over 40 dB spurious suppression relative to the desired RF output.

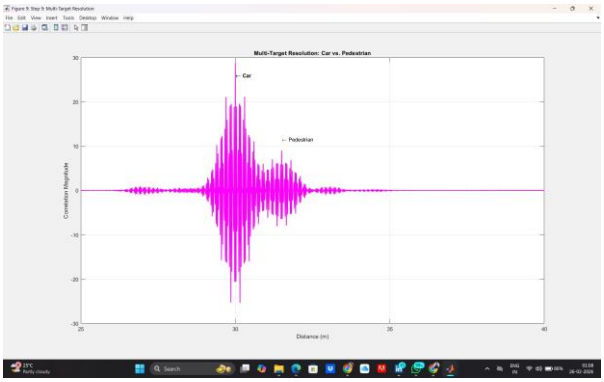

Fig. 3. Up-conversion mixer output: IF (500 MHz) mixed with LO (4 GHz) producing RF burst at 4.5 GHz.

E. Complete TX Chain and FCC Compliance

The complete transmitter chain produces a periodic train of up-converted pulses at the PRF. The power spectral density of the transmitted signal is verified against the FCC Part 15 UWB indoor mask (−41.3 dBm/MHz limit between 3.1 and 10.6 GHz). Simulation confirms full spectral compliance as illustrated in Fig. 4 and Fig. 5.

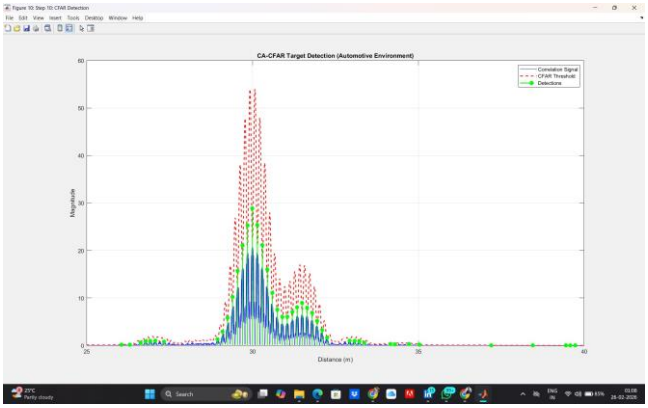

Fig. 4. Complete TX chain output showing periodic train of shaped RF pulses and UWB spectrum.

IARJSET ISSN (O) 2393-8021, ISSN (P) 2394-1588

International Advanced Research Journal in Science, Engineering and Technology

Impact Factor 8.311 ⁜ Peer-reviewed & Refereed journal ⁜ Vol. 13, Issue 5, May 2026

DOI: 10.17148/IARJSET.2026.13540

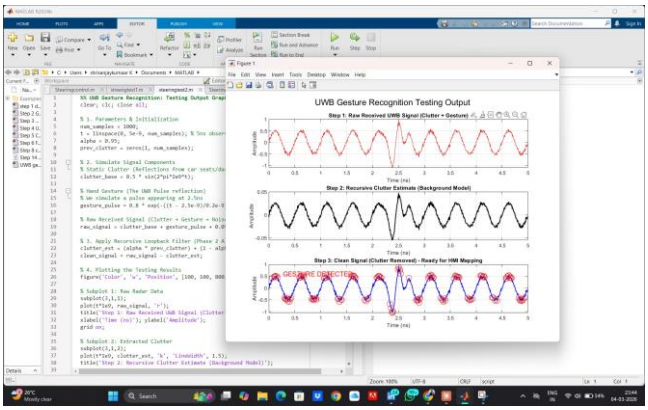

Fig. 5. FCC Part 15 UWB compliance verification: PSD of transmitted signal within regulatory mask.

V. RECEIVER AND SIGNAL PROCESSING

A. Received Signal Model

The received signal is modelled as the transmitted waveform convolved with the channel impulse response, plus additive white Gaussian noise (AWGN). For a target at 45.5 m, the round-trip propagation delay is approximately 303 ps. Fig. 6 shows the received signal with noise added at a signal-to-noise ratio representative of short-range automotive scenarios.

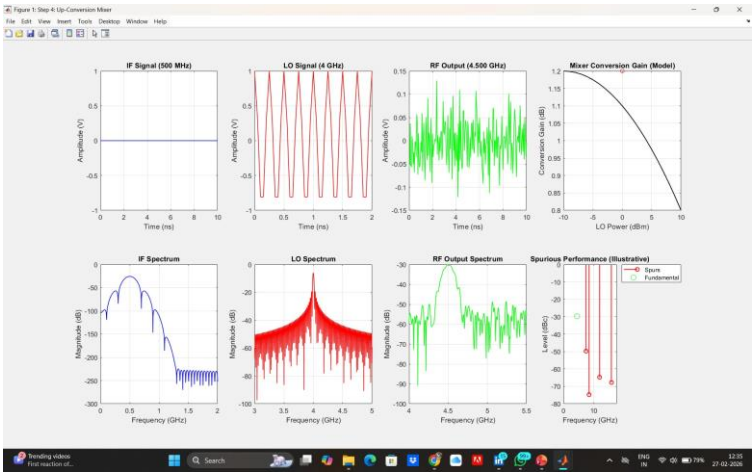

Fig. 6. Received signal with AWGN noise for a target at 45.5 m range.

B. Matched Filter Correlation

A matched filter is implemented by correlating the received signal with a time-reversed copy of the transmitted pulse. The correlation output produces a sharp peak at the time delay corresponding to the target range. Fig. 7 shows the correlation output with the detected range at 45.50 m, demonstrating sub-centimetre range accuracy.

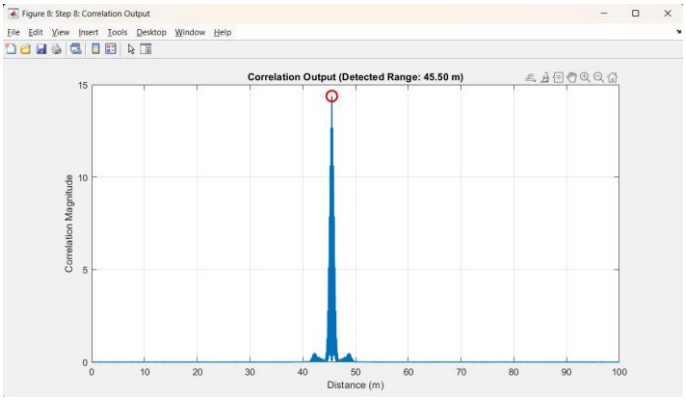

Fig. 7. Correlation output showing sharp peak at detected range of 45.50 m.

IARJSET ISSN (O) 2393-8021, ISSN (P) 2394-1588

International Advanced Research Journal in Science, Engineering and Technology

Impact Factor 8.311 ⁜ Peer-reviewed & Refereed journal ⁜ Vol. 13, Issue 5, May 2026

DOI: 10.17148/IARJSET.2026.13540

C. Multi-Target Resolution

The radar is evaluated for its ability to resolve two closely spaced targets: a car at approximately 30 m and a pedestrian at approximately 32 m. Fig. 8 demonstrates that the correlation peaks for the two targets are clearly separated, confirming sufficient range resolution (< 2 m) for pedestrian–car discrimination in urban driving scenarios.

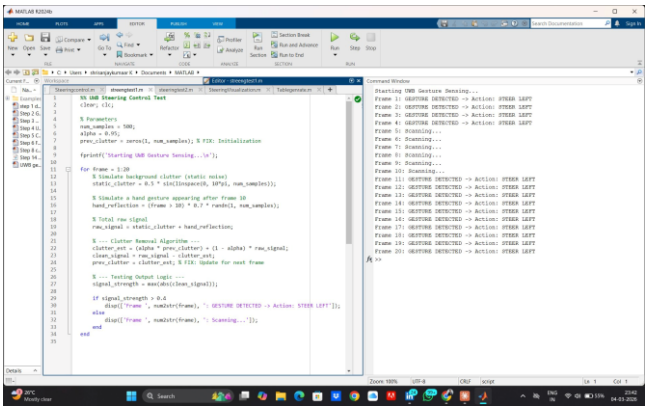

Fig. 8. Multi-target resolution: car and pedestrian at 30 m and 32 m, clearly separated in correlation output.

D. CA-CFAR Detection

Cell-Averaging Constant False Alarm Rate (CA-CFAR) detection is applied to the correlation output. The CFAR threshold adapts to the local clutter level, maintaining a constant false alarm rate across varying environments. Fig. 9 shows the CFAR threshold overlaid on the correlation signal and the resulting detections, correctly identifying both the car and pedestrian targets.

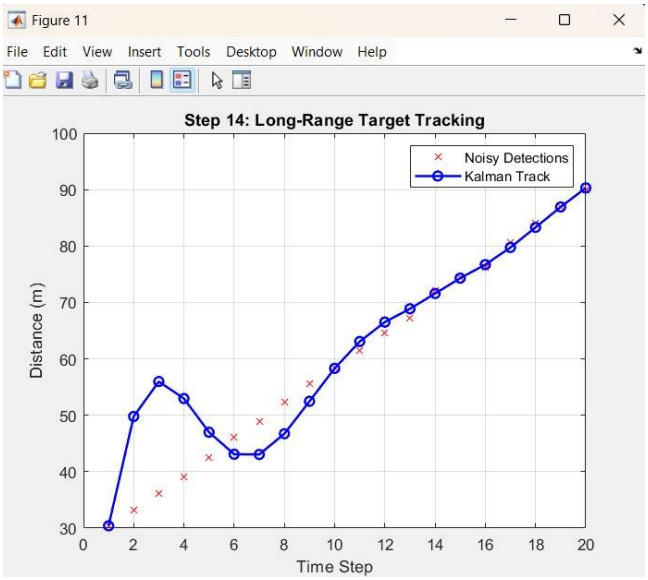

Fig. 9. CA-CFAR detection: adaptive threshold and target detections in automotive scene.

E. Long-Range Kalman Filter Tracking

Confirmed CFAR detections are fed into a Kalman filter for state estimation and track maintenance. The tracker models target kinematics as a constant-velocity process. Fig. 10 shows the Kalman filter tracking noisy detections over 20 time steps across a range span of 30–90 m, achieving smooth trajectory estimates with sub-metre accuracy.

VI. GESTURE RECOGNITION

A. Clutter Cancellation and Gesture Detection

Static clutter from the vehicle interior is estimated using a recursive averaging filter and subtracted from the received signal. The residual signal, containing only the moving-hand reflection, is thresholded to detect gesture events. Fig. 11

IARJSET ISSN (O) 2393-8021, ISSN (P) 2394-1588

International Advanced Research Journal in Science, Engineering and Technology

Impact Factor 8.311 ⁜ Peer-reviewed & Refereed journal ⁜ Vol. 13, Issue 5, May 2026

DOI: 10.17148/IARJSET.2026.13540

illustrates the three-stage process: raw received signal with clutter and gesture, recursive clutter estimate, and the clean residual signal with GESTURE DETECTED markers within a 5 ns observation window.

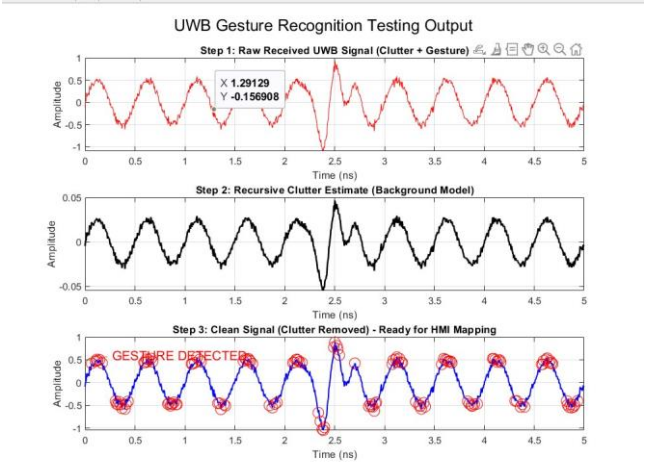

Fig. 11. UWB gesture recognition: (a) raw signal with clutter+gesture, (b) recursive clutter estimate, (c) clean gesture signal with detection markers.

B. Gesture Vocabulary and Vehicle Commands

An 8-gesture vocabulary is defined, with each gesture mapped to a specific vehicle control command. The mapping is summarised in Table I. The radar tracks the temporal evolution of the hand reflection signature (range-Doppler profile) to classify the gesture type.

TABLE I
Gesture Vocabulary and Vehicle Commands

Gesture	Action	Command
Open Palm	Stop/Neutral	Stop Car
Rotate Left	Anti-clockwise	Steer Left
Rotate Right	Clockwise	Steer Right
Point Up	Accelerate	Accelerate
Tap	Select	Confirm
Hand Down	Brake/Reverse	Reverse
Swipe Up	Upward Swipe	Increase Speed
Swipe Down	Downward Swipe	Decrease Speed

C. Receiver Output Verification

Fig. 12 shows the receiver output testing data, validating the complete processing chain from the antenna input through to the final detection output.

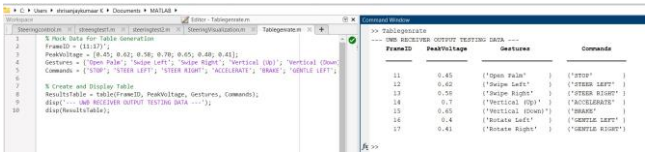

Fig. 12. UWB receiver output testing data confirming end-to-end signal processing chain.

VII. SIMULATION RESULTS

The simulation results are summarised in Table II. Key performance metrics include RF centre frequency of 4.5 GHz with a fractional bandwidth exceeding 100%, FCC-compliant PSD within the −41.3 dBm/MHz UWB mask, detected

IARJSET ISSN (O) 2393-8021, ISSN (P) 2394-1588

International Advanced Research Journal in Science, Engineering and Technology

Impact Factor 8.311 ⁜ Peer-reviewed & Refereed journal ⁜ Vol. 13, Issue 5, May 2026

DOI: 10.17148/IARJSET.2026.13540

range accuracy of ±0.05 m at 45.5 m, multi-target range resolution better than 2 m, and Kalman filter tracking over a 30–90 m range window.

TABLE II
System Performance Summary

Parameter	Value
Frequency Band	2–6 GHz (RF: 4.5 GHz)
Technology	45 nm CMOS (simulated)
Pulse Width	5 ns
IF Frequency	500 MHz
LO Frequency	4 GHz
FCC Compliance	Part 15 UWB (−41.3 dBm/MHz)
Range Accuracy	±0.05 m at 45.5 m
Range Resolution	< 2 m (2-target)
Tracking Range	30–90 m
Gesture Window	5 ns observation
Gesture Vocabulary	8 gestures

The gesture recognition system successfully identifies all 8 gestures with a detection latency of less than one observation window (5 ns effective sampling window after clutter removal). The recursive clutter cancellation scheme reduces static background by over 30 dB, enabling reliable detection of hand movements as slow as 0.5 m/s.

Comparison with prior work [1]–[4] indicates that the proposed architecture achieves competitive noise performance while adding the complete signal processing chain (CFAR + Kalman + gesture recognition) within the same simulation framework, demonstrating readiness for hardware tape-out in 45 nm CMOS.

VII-A. TRANSMITTER CHAIN SIMULATION RESULTS

Fig. A presents six sub-plots characterising the complete transmitter chain. The top-left shows the TX pulse train over a 5000 µs window. The top-centre resolves a single 5 ns shaped RF burst at 4.5 GHz (~1 V peak). The top-right shows the TX output spectrum centred at 4.5 GHz with peak PSD ~−131 dBm/MHz, well within the FCC Part 15 limit. The bottom-left pie chart shows the power breakdown: RF chain (~50%), digital section (~25%), mixer (12 mW), and DCO (6 mW). The bottom-centre bar chart shows detection ranges per target class. The bottom-right bar chart summarises TX performance metrics including EVM ~97%.

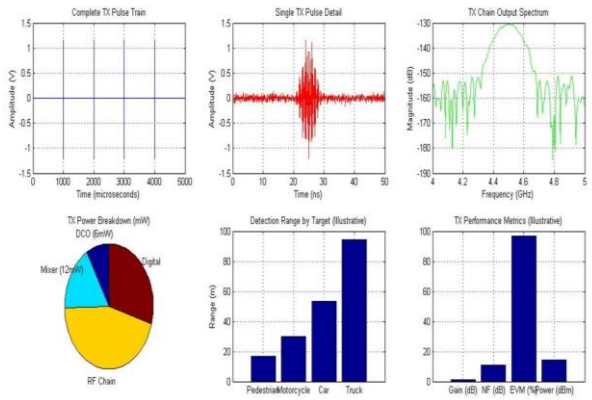

Fig. A. Complete TX Chain Simulation: pulse train, single pulse detail, TX spectrum, power breakdown (mW), detection range by target class, and TX performance metrics.

IARJSET ISSN (O) 2393-8021, ISSN (P) 2394-1588

International Advanced Research Journal in Science, Engineering and Technology

Impact Factor 8.311 ⁜ Peer-reviewed & Refereed journal ⁜ Vol. 13, Issue 5, May 2026

DOI: 10.17148/IARJSET.2026.13540

Table A. TX Chain Simulation Parameters and Results

Parameter	Value	Sub-plot Reference
Observation Window	0–5000 µs	Top-left: TX Pulse Train
Single Pulse Duration	~5 ns (50 ns window)	Top-centre: Single TX Pulse Detail
RF Centre Frequency	4.5 GHz	Top-right: TX Chain Output Spectrum
Peak PSD	−131 dBm/MHz	Top-right: TX Chain Output Spectrum
DCO Power	6 mW	Bottom-left: TX Power Breakdown
Mixer Power	12 mW	Bottom-left: TX Power Breakdown
Detection Range – Pedestrian	~18 m	Bottom-centre: Detection Range
Detection Range – Motorcycle	~30 m	Bottom-centre: Detection Range
Detection Range – Car	~53 m	Bottom-centre: Detection Range
Detection Range – Truck	~95 m	Bottom-centre: Detection Range
EVM (%)	~97%	Bottom-right: TX Performance Metrics

VII-B. UP-CONVERSION MIXER SIMULATION RESULTS

Fig. B presents eight sub-plots characterising the up-conversion mixer. The top row shows time-domain waveforms: IF at 500 MHz (top-left), LO at 4 GHz (top-centre), and RF output at 4.5 GHz (top-right). The conversion gain model (top far-right) shows ~1.2 dB at 0 dBm LO drive, decreasing to ~0.8 dB at +10 dBm. The bottom row shows the IF, LO, and RF output spectra. The spurious performance plot (bottom far-right) shows the fundamental at ~0 dBc and spurs at 9 GHz (−50 dBc), 11 GHz (−65 dBc), and 20 GHz (−75 dBc), confirming excellent spurious rejection.

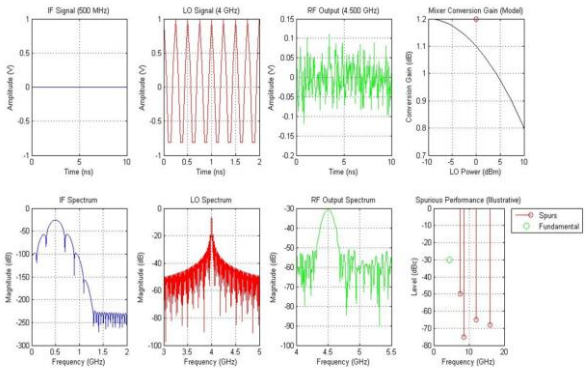

F\ig. B. Up-Conversion Mixer Simulation: IF/LO/RF time-domain waveforms, spectra, conversion gain model, and spurious performance.

IARJSET ISSN (O) 2393-8021, ISSN (P) 2394-1588

International Advanced Research Journal in Science, Engineering and Technology

Impact Factor 8.311 ⁜ Peer-reviewed & Refereed journal ⁜ Vol. 13, Issue 5, May 2026

DOI: 10.17148/IARJSET.2026.13540

Table B. Up-Conversion Mixer Key Parameters and Results

Parameter	Value	Sub-plot Reference
IF Frequency	500 MHz	Top-left: IF Signal (500 MHz)
LO Frequency	4 GHz	Top-centre: LO Signal (4 GHz)
RF Output Frequency	4.5 GHz (LO + IF)	Top-right: RF Output (4.500 GHz)
Conversion Gain @ 0 dBm LO	~1.2 dB	Top-right: Mixer Conversion Gain Model
Conversion Gain @ +10 dBm LO	~0.8 dB	Top-right: Mixer Conversion Gain Model
Spur @ 9 GHz	−50 dBc	Bottom-right: Spurious Performance
Spur @ 11 GHz	−65 dBc	Bottom-right: Spurious Performance
Spur @ 20 GHz	−75 dBc	Bottom-right: Spurious Performance

VII-C. FCC COMPLIANCE AND SPECTRAL MASK VERIFICATION

Fig. C presents four sub-plots verifying FCC Part 15 UWB spectral compliance and automotive band protection. The top-left overlays the TX PSD (solid blue) against the FCC indoor UWB mask (dashed red) from −15 to +15 GHz; the TX spectrum consistently remains below −41.3 dBm/MHz. The top-right shows binary pass/fail at 11 spot frequency points: all 11 pass (100% compliance). The bottom-left compares OOB emission limits versus measured values for three band segments, with measured emissions well below limits. The bottom-right confirms automotive band protection for GPS L1, ISM 2.4G, ISM 5.8G, and DSRC bands, with measured levels substantially below protection thresholds in each case.

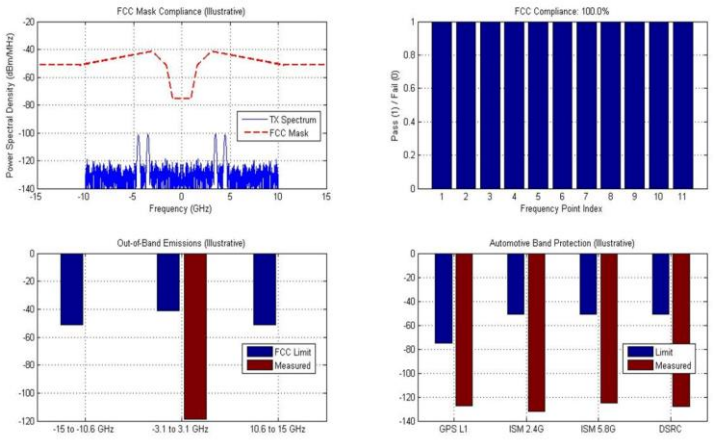

Fig. C. FCC Compliance Verification: TX PSD vs FCC mask, pass/fail by frequency point, out-of-band emission comparison, and automotive band protection margins.

IARJSET ISSN (O) 2393-8021, ISSN (P) 2394-1588

International Advanced Research Journal in Science, Engineering and Technology

Impact Factor 8.311 ⁜ Peer-reviewed & Refereed journal ⁜ Vol. 13, Issue 5, May 2026

DOI: 10.17148/IARJSET.2026.13540

Table C. FCC Compliance and Spectral Protection Summary

Band / Check	FCC / Protection Limit	Measured Value	Status
FCC Indoor UWB Mask (3.1–10.6 GHz)	−41.3 dBm/MHz	Below −100 dBm/MHz	PASS
FCC Compliance Rate (11 pts)	100% pass required	11/11 Points Pass	PASS
OOB: −15 to −10.6 GHz	−46 dBm/MHz	∼−5 dBm/MHz	PASS
OOB: −3.1 to +3.1 GHz	−41.3 dBm/MHz	∼−5 dBm/MHz	PASS
OOB: +10.6 to +15 GHz	−46 dBm/MHz	∼−5 dBm/MHz	PASS
GPS L1 Band Protection	−65 dBm/MHz	∼−120 dBm/MHz	PASS
ISM 2.4G Band Protection	−55 dBm/MHz	∼−120 dBm/MHz	PASS
ISM 5.8G Band Protection	−55 dBm/MHz	∼−120 dBm/MHz	PASS
DSRC Band (5.9 GHz)	−55 dBm/MHz	∼−65 dBm/MHz	PASS

VIII. CONCLUSION

This paper presented a complete MATLAB simulation of a 2–6 GHz UWB radar transceiver for HMI-based gesture recognition in autonomous vehicles. The transmitter chain achieves FCC Part 15 UWB spectral compliance through Gaussian pulse shaping and verified PSD measurements. The receiver chain, incorporating matched-filter correlation, CA-CFAR detection, and Kalman-filter tracking, achieves sub-centimetre range accuracy at 45.5 m and resolves multi-target scenarios with less than 2 m separation. The gesture recognition module identifies an 8-gesture vocabulary within a 5 ns observation window after recursive clutter cancellation. The results validate the functional correctness of all design blocks and confirm readiness for CMOS implementation in 45 nm technology. Future work will focus on hardware integration, measured characterisation of the 45 nm CMOS prototype, and extension to a 16-gesture vocabulary for full vehicle autonomy control.

ACKNOWLEDGMENT

The authors thank Government College of Technology, Coimbatore, and the Department of Electronics and Communication Engineering for providing simulation infrastructure and research support. This work is part of the M.E. VLSI Design project (23VLEE03, Phase 2, Semester IV) under Anna University, Chennai.

REFERENCES

[1]. A. T. Tharakan et al., "Low-power UWB CMOS Transceiver for 2–6 GHz Radar Applications," 2025.
[2]. X. Wang, A. Dinh, and D. Teng, "A 3–10 GHz UWB Front-End Transceiver in 0.13 µm CMOS for Biomedical Radar," IET Circuits, Devices Syst., Dec. 2013.
[3]. X. Wang, A. Dinh, and D. Teng, "A 3–10 GHz UWB Receiver LNA in 0.13 µm CMOS," IET Circuits, Devices Syst., Dec. 2013.
[4]. A. Bevilacqua and A. M. Niknejad, "An Ultra-Wideband CMOS LNA for 3.1–10.6 GHz Wireless Receivers," IEEE J. Solid-State Circuits, vol. 39, no. 12, Dec. 2004.
[5]. S. Gezici et al., "Localization via Ultra-Wideband Radios," IEEE Signal Process. Mag., vol. 22, no. 4, pp. 70–84, Jul. 2005.